Available online at www.sciencedirect.com
ScienceDirect
Trans. Nonferrous Met. Soc. China 23(2013) 1090−1097
Transactions of Nonferrous Metals Society of China
www.tnmsc.cn

Theoretical prediction of effective elastic constants for new intermetallic compound porous material

Shu-lan SU[1,2], Qiu-hua RAO[1], Yue-hui HE[3]

1. School of Civil Engineering, Central South University, Changsha 410075, China;
2. College of Civil Engineering and Mechanics, Central South University of Forestry & Technology, Changsha 410004, China;
3. Powder Metallurgy Research Institute, Central South University, Changsha 410083, China

Received 16 March 2012; accepted 8 January 2013

Abstract: Based on microstructure analysis of the new Ti−Al intermetallic compound porous material, a micromechanics model of heterogeneous Plateau porous structure was established and calculation formulas of elastic constants (including effective elastic modulus, effective shear elastic modulus and effective Poisson ratio) were derived by the energy method for this porous material. Calculation results show that both the effective elastic modulus and effective shear elastic modulus increase with the increase of the relative density while the effective Poisson ratio decreases. Compared with the currently-existing hexagonal honeycomb model and micromechanics model of composite materials, the micromechanics model of heterogeneous Plateau porous structure in this study is more suitable for characterizing the medium-density porous material and more accurate for predicting the effective elastic constants of the medium-density porous material. Moreover, the obtained explicit expressions of the effective elastic constants in term of the relative density rather than the microstructural parameters for the uniform and regular Plateau porous structure are more convenient to engineering application.

Key words: intermetallic compound; porous material; effective elastic modulus; Plateau structure; energy method

1 Introduction

Porous material has been widely used in medicine, chemical industry, metallurgy, environmental protection, aerospace and building engineering, owing to its special performance of large specific surface area, high specific mechanical properties, good damping properties and large adsorption capacity, and a variety of functions such as filtration, separation, adsorption, sound-insulation and anti-seism [1−6]. Ti−Al intermetallic compound is a kind of structural material with light weight, high strength and high temperature resistance, but its potential chemical, physical and mechanical properties have not been fully developed. Recently, our research group proposed a new method of element mixture partial diffusion−reactive synthesis−sintering to successfully prepare the Ti−Al intermetallic compound porous material [7], which has advantages of both ceramic and metal porous materials, with higher specific strength and specific modulus, better resistance to high temperature and oxidation [8]. It will be a promising structure and filter material of light weight and high strength.

It is well known that mechanical properties of the porous materials strongly depend on its relative density, pore structure morphology and properties of solid materials. For the low-density porous material of the relative density less than 0.3 (i.e., $0<\rho^*/\rho_s<0.3$, where ρ^* and ρ_s are densities of porous and solid materials, respectively), it is usually simplified as interconnected holes or obturator network structure in study of its mechanical properties [9−13]. Elastic mechanics [14] or mechanics of composite material [15,16] is used to study the mechanical properties of the high-density porous material with the relative density larger than 0.8 (i.e., $\rho^*/\rho_s>0.8$). Ti−Al intermetallic compound porous material prepared by the reaction synthesis is of medium density (i.e., $0.3<\rho^*/\rho_s<0.8$). Due to its complexity and heterogeneity of microscopic structure, analytically characterizing the mechanical properties of the

Foundation item: Project (50825102) supported by the National Natural Science Funds for Distinguished Young Scholar, China; Project (2009CB623406) supported by the National Basic Research Program of China
Corresponding author: Qiu-hua RAO; Tel: +86-13787265488; E-mail: raoqh@mail.csu.edu.cn
DOI: 10.1016/S1003-6326(13)62570-4

medium density porous materials becomes one of the hot and difficult issues in preparation and application of this new material.

In this study, a meso-mechanical model of Plateau porous structure was established based on microstructure analysis of the new Ti−Al intermetallic compound porous material. Calculation formulas of the effective elastic constants (including effective elastic modulus, effective shear elastic modulus and effective Poisson ratio) were derived by the energy method in order to provide theoretical basis for predicting the mechanical properties of the medium-density porous material.

2 Meso-mechanical model of porous structure

The new Ti−Al intermetallic compound porous material is a kind of porous skeleton structure prepared by the three-stage sintering process with characteristics of solid reaction and partial diffusion. It has mostly open pore structure of high relative density (Fig. 1) and can be considered Plateau porous structure [11] with the meso-mechanics model shown in Fig. 2(a). The Plateau porous structure consists of four inclined struts of length (l) and two vertical struts of length (h). In the space coordinate system, the angle between the inclined strut and X_1 axis is θ and the thickness of structure in X_3 direction is b, smaller than l or h. Because of structural symmetry, the shadow part in Fig. 2(a) is selected to be the representative unit and its detailed size is shown in Fig. 2(b). The geometry size as well as the force and deformation of each strut is symmetrical about its midpoint. It is assumed the strut is isotropic and linear elastic material and the elastic modulus of material is E_s.

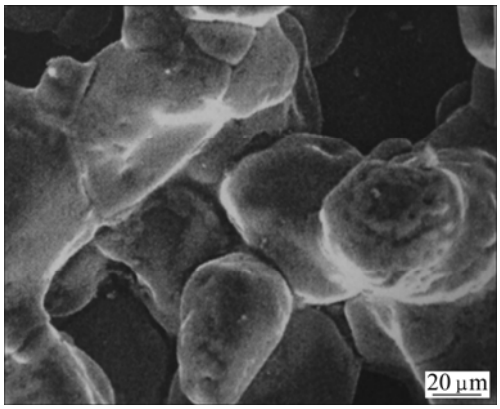

Fig. 1 SEM image of Ti−Al intermetallic compound porous material

The effective elastic constants (including the effective elastic modulus E_1^* and E_2^*, the effective shear modulus G_{12}^* and the effective Poisson ratio μ_{12}^*) can be determined based on the displacement, s, of

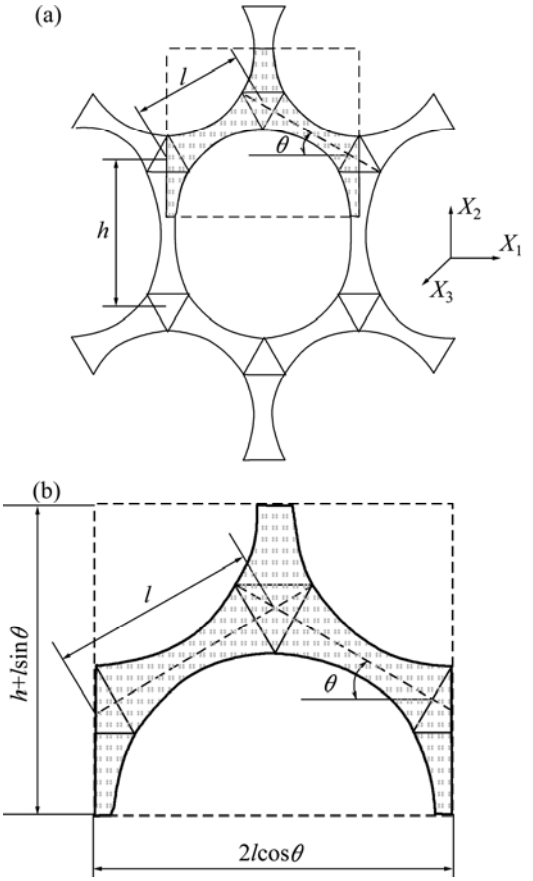

Fig. 2 Meso-mechanics model of porous structure: (a) Plateau porous structure; (b) Representative unit

the representative unit in X_1−X_2 plane calculated by energy method as follows [17]:

$$\Delta=\sum\int\frac{N\cdot\bar{N}}{EA}\mathrm{d}s+\sum\int\frac{k\cdot Q\cdot\bar{Q}}{GA}\mathrm{d}s+\sum\int\frac{M\cdot\bar{M}}{EI}\mathrm{d}s \quad (1)$$

where N, Q and M are axial force, shear and bending moment caused by actual load, respectively; $\bar{N}$, $\bar{Q}$ and $\bar{M}$ are axial force, shear and bending moment caused by virtual unit load, respectively; k is a shear correction coefficient depending on the cross section of the strut.

3 Prediction of effective elastic constants

3.1 Effective elastic modulus E_1^* and E_2^*

For calculating E_1^* in X_1 direction, the representative unit is subject to a uniform tensile stress σ_1, as shown in Fig. 3(a), and its resultant force in the X_1 direction is $F_1=\sigma_1 b(h+l\sin\theta)$. The actual internal forces of the inclined strut are $N_l=F_1\cos\theta$, $Q_l=F_1\sin\theta$ and $M_l=F_1 x\sin\theta$, respectively. When a unit load is applied to the representative unit, i.e., $F_1=1$, the virtual internal forces of the inclined strut become $\bar{N}_l=\cos\theta$, $\bar{Q}_l=\sin\theta$ and $\bar{M}_l=x\sin\theta$, respectively. No internal force exists in the vertical strut.

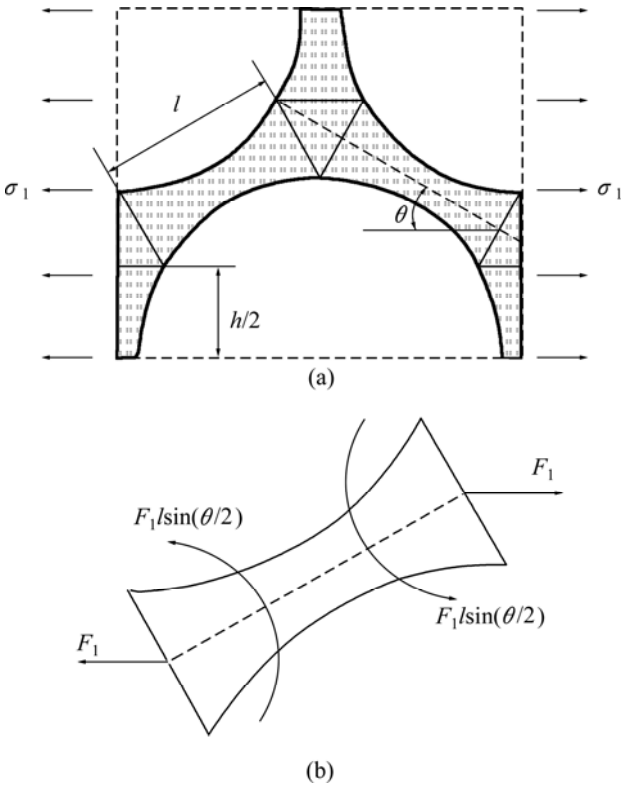

Fig. 3 Representative unit subjected to a uniform tensile stress σ_1 in X_1 direction: (a) Representative unit; (b) Inclined strut

The X_1-directional displacement of the inclined strut, Δ_{l1}, is obtained by substituting the actual and virtual internal forces of the inclined strut into Eq. (1):

$$\Delta_{l1}=2F_1\cos^2\theta\int_0^{l/2}\frac{\mathrm{d}x}{E_sA_l(x)}+4k(1+\mu)\cdot F_1\sin^2\theta\int_0^{l/2}\frac{\mathrm{d}x}{E_sA_l(x)}+2F_1\sin^2\theta\int_0^{l/2}\frac{x^2\mathrm{d}x}{E_sI_l(x)}$$

Due to the structural symmetry, the X_1-directional displacement of the unit is $\Delta_1=2\Delta_{l1}$, i.e.,

$$\Delta_1=4F_1\cos^2\theta\int_0^{l/2}\frac{\mathrm{d}x}{E_sA_l(x)}+8k(1+\mu)\cdot F_1\sin^2\theta\int_0^{l/2}\frac{\mathrm{d}x}{E_sA_l(x)}+4F_1\sin^2\theta\int_0^{l/2}\frac{x^2\mathrm{d}x}{E_sI_l(x)} \quad (2)$$

The X_1-directional linear strain of the unit, ε_1, is given by

$$\varepsilon_1=\frac{\Delta_1}{2l\cos\theta} \quad (3)$$

Therefore, the effective elastic modulus E_1^* along the X_1 direction is calculated as follows:

$$E_1^*=\frac{\sigma_1}{\varepsilon_1}=\frac{l\cos\theta}{2b(h+l\sin\theta)}\cdot1\Big/\left[\cos^2\theta\int_0^{l/2}\frac{\mathrm{d}x}{E_sA_l(x)}+2k(1+\mu)\sin^2\theta\int_0^{l/2}\frac{\mathrm{d}x}{E_sA_l(x)}+\sin^2\theta\int_0^{l/2}\frac{x^2\mathrm{d}x}{E_sI_l(x)}\right] \quad (4)$$

Similarly, the effective elastic modulus E_2^* along the X_2 direction is given by

$$E_2^*=\frac{\sigma_2}{\varepsilon_2}=\frac{h+l\sin\theta}{2bl\cos\theta}\cdot1\Big/\left[\sin^2\theta\int_0^{l/2}\frac{\mathrm{d}x}{E_sA_l(x)}+2k(1+\mu)(\cos^2\theta\int_0^{l/2}\frac{\mathrm{d}x}{E_sA_l(x)}+\cos^2\theta\int_0^{l/2}\frac{x^2\mathrm{d}x}{E_sI_l(x)}+2\int_0^{h/2}\frac{\mathrm{d}x}{E_sA_h(x)}\right] \quad (5)$$

3.2 Effective shear modulus G_{12}^*

For calculating G_{12}^* in X_1 direction, the representative unit is subject to a uniform shear stress τ_{12} in X_1−X_2 plane (Fig. 4). Its shear strain in the X_1−X_2 plane is the sum of the shear strain in the X_1 and X_2 directions, i.e., $\gamma_{12}=\gamma_a+\gamma_b$. The resultant forces in the X_1 and X_2 directions are $F_1=2\tau_{12}bl\cos\theta$ and $F_2=\tau_{12}b(h+l\sin\theta)$, as shown in Fig. 5. Therefore, the internal forces of the inclined strut l are $N_l=F_2\sin\theta+F_1\cos(\theta/2)$, $Q_l=F_2\cos\theta-F_1\sin(\theta/2)$ and $M_l=(F_2\cos\theta-F_1\sin(\theta/2))\cdot x$. The internal forces of the vertical strut h are $N_h=0$, $Q_h=F_1$ and $M_h=F_1\cdot x$.

When a unit load ($F_1=1$) is applied to the representative unit in the X_1 direction, the virtual internal forces of the inclined strut l and the vertical strut h are $\bar{N}_l=\cos(\theta/2)$, $\bar{Q}_l=-\sin(\theta/2)$, $\bar{M}_l=-x/2\sin\theta$ and $\bar{N}_h=0$, $\bar{Q}_h=1$, $\bar{M}_h=x$, respectively.

According to Eq. (1), the displacements of the inclined strut l and the vertical strut h in X_1 direction can be obtained:

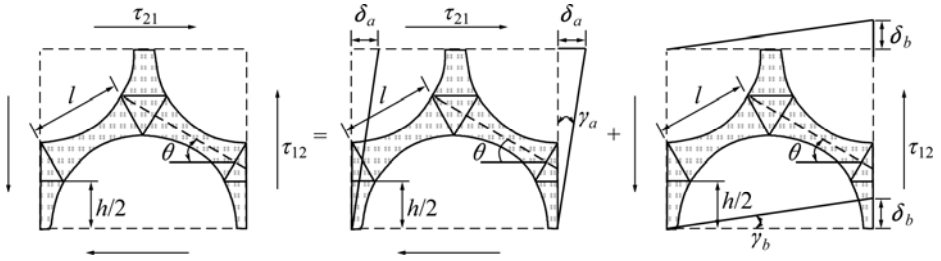

Fig. 4 Representative unit subjected to a uniform shear stress τ_{12} in X_1−X_2 plane

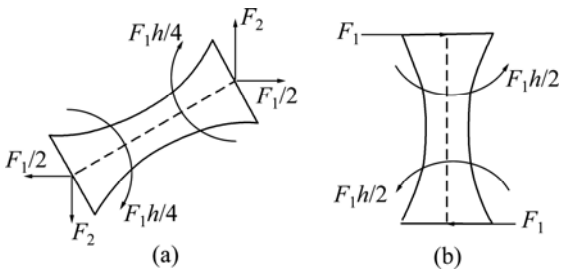

Fig. 5 Force analyses of inclined strut l and vertical strut h: (a) Inclined strut l; (b) Vertical strut h

$$\delta_{al}=2(F_2\sin\theta+\frac{1}{2}F_1\cos\theta)\cos\theta\cdot\int_0^{l/2}\frac{\mathrm{d}x}{E_sA_l(x)}-$$
$$4k(1+\mu)(F_2\cos\theta-\frac{1}{2}F_1\sin\theta)\sin\theta\cdot\int_0^{l/2}\frac{\mathrm{d}x}{E_sA_l(x)}-$$
$$2(F_2\cos\theta-\frac{1}{2}F_1\sin\theta)\sin\theta\cdot\int_0^{l/2}\frac{x^2\mathrm{d}x}{E_sI_l(x)}$$
$$\delta_{ah}=4k(1+\mu)F_1\cdot\int_0^{h/2}\frac{\mathrm{d}x}{E_sA_h(x)}+2F_1\cdot\int_0^{h/2}\frac{x^2\mathrm{d}x}{E_sI_h(x)}$$

The displacement of the unit in X_1 direction is $\delta_a=\delta_{al}+\delta_{ah}$, i.e.,

$$\delta_a=2(F_2\sin\theta+\frac{1}{2}F_1\cos\theta)\cos\theta\cdot\int_0^{l/2}\frac{\mathrm{d}x}{E_sA_l(x)}-$$
$$4k(1+\mu)(F_2\cos\theta-\frac{1}{2}F_1\sin\theta)\sin\theta\cdot\int_0^{l/2}\frac{\mathrm{d}x}{E_sA_l(x)}-$$
$$2(F_2\cos\theta-\frac{1}{2}F_1\sin\theta)\sin\theta\cdot\int_0^{l/2}\frac{x^2\mathrm{d}x}{E_sI_l(x)}+$$
$$4k(1+\mu)F_1\cdot\int_0^{h/2}\frac{\mathrm{d}x}{E_sA_h(x)}+2F_1\cdot\int_0^{h/2}\frac{x^2\mathrm{d}x}{E_sI_h(x)}\quad(6)$$

Similarly, the displacement of the unit in X_2 direction is

$$\delta_b=4(F_2\sin\theta+\frac{1}{2}F_1\cos\theta)\sin\theta\int_0^{l/2}\frac{\mathrm{d}x}{E_sA_l(x)}+$$
$$4(F_2\cos\theta-\frac{1}{2}F_1\sin\theta)\cos\theta\int_0^{l/2}\frac{x^2\mathrm{d}x}{E_sI_l(x)}+$$
$$8k(1+\mu)(F_2\cos\theta-\frac{1}{2}F_1\sin\theta)\cos\theta\int_0^{l/2}\frac{\mathrm{d}x}{E_sA_l(x)}\quad(7)$$

The shear strain γ_{12} of the unit in X_1–X_2 plane is given by

$$\gamma_{12}=\gamma_a+\gamma_b=\frac{\delta_a}{h+l\sin\theta}+\frac{\delta_b}{2l\cos\theta}\quad(8)$$

Substituting Eqs. (6) and (7) into Eq. (8) results in the effective shear modulus G_{12}^* as follows:

$$G_{12}^*=\frac{\tau_{12}}{\gamma_{12}}=\frac{l\cos\theta(h+l\sin\theta)}{2b}\times$$
$$\left[\cos^2\theta\left(h^2\int_0^{l/2}\frac{x^2\mathrm{d}x}{E_sI_l(x)}+2l^2\int_0^{h/2}\frac{x^2\mathrm{d}x}{E_sI_h(x)}\right)+\right.$$
$$(l+h\sin\theta)^2\int_0^{l/2}\frac{\mathrm{d}x}{E_sA_l(x)}+2k(1+\mu)\cdot$$
$$\left.\cos^2\theta\left(h^2\int_0^{l/2}\frac{\mathrm{d}x}{E_sA_l(x)}+2l^2\int_0^{h/2}\frac{\mathrm{d}x}{E_sA_h(x)}\right)\right]^{-1}\quad(9)$$

3.3 Effective Poisson ratios μ_{12}^* and μ_{21}^*

The effective Poisson ratio μ_{12}^* can be calculated by the X_1-directional linear strain ε_1 shown in Eq. (3) and the X_2-directional linear strain ε_1' caused by σ_1.

According to the energy method, the X_2-directional linear displacement Δ_{12} and linear strain ε_1' caused by σ_1 are

$$\Delta_{12}=2\int_0^{l}\frac{F_1\cos\theta\sin\theta}{2E_sA_l(x)}\mathrm{d}x-2\int_0^{l}\frac{k\cdot F_1\sin\theta\cos\theta}{2GA_l(x)}\mathrm{d}x-$$
$$2\int_0^{l}\frac{F_1x^2\sin\theta\cos\theta}{2E_sI_l(x)}\mathrm{d}x=$$
$$2F_1\cos\theta\sin\theta\int_0^{l/2}\frac{\mathrm{d}x}{E_sA_l(x)}-$$
$$4k(1+\mu)\cdot F_1\sin\theta\cos\theta\int_0^{l/2}\frac{\mathrm{d}x}{E_sA_l(x)}-$$
$$2F_1\sin\theta\cos\theta\int_0^{l/2}\frac{x^2\mathrm{d}x}{E_sI_l(x)}\quad(10)$$

$$\varepsilon_1'=\frac{\Delta_{12}}{h+l\sin\theta}\quad(11)$$

Therefore, the effective Poisson ratio μ_{12}^* caused by σ_1 is

$$\mu_{12}^*=-\frac{\varepsilon_1'}{\varepsilon_1}=-\{l\cos^2\theta\sin\theta[\int_0^{l/2}\frac{\mathrm{d}x}{E_sA_l(x)}-$$
$$2k(1+\mu)\int_0^{l/2}\frac{\mathrm{d}x}{E_sA_l(x)}-\int_0^{l/2}\frac{x^2\mathrm{d}x}{E_sI_l(x)}]\}/$$
$$\{(h+l\sin\theta)[\cos^2\theta\int_0^{l/2}\frac{\mathrm{d}x}{E_sA_l(x)}+$$
$$2k(1+\mu)\sin^2\theta\int_0^{l/2}\frac{\mathrm{d}x}{E_sA_l(x)}+\sin^2\theta\int_0^{l/2}\frac{x^2\mathrm{d}x}{E_sI_l(x)}]\}\quad(12)$$

Similarly, the effective Poisson ratio μ_{12}^* caused by σ_2 is

$$\mu_{21}^*=-\frac{(h+l\sin\theta)\sin\theta}{l}\cdot\left[\int_0^{l/2}\frac{\mathrm{d}x}{E_sA_l(x)}-\right.$$
$$2k(1+\mu)\int_0^{l/2}\frac{\mathrm{d}x}{E_sA_l(x)}-\int_0^{l/2}\frac{x^2\mathrm{d}x}{E_sI_l(x)})/$$
$$[\sin^2\theta\int_0^{l/2}\frac{\mathrm{d}x}{E_sA_l(x)}+2k(1+\mu)\cos^2\theta\int_0^{l/2}\frac{\mathrm{d}x}{E_sA_l(x)}+$$

$$\cos^2\theta\int_0^{l/2}\frac{x^2\mathrm{d}x}{E_s I_l(x)}+2\int_0^{h/2}\frac{\mathrm{d}x}{E_s A_h(x)}\Bigg] \tag{13}$$

4 Verification

4.1 Effective elastic constants of non-uniform and regular Plateau porous structure

Equations (4), (5), (9), (12) and (13) are calculation formulas for effective elastic constants of the non-uniform and non-regular Plateau porous structure.

For the non-uniform and regular Plateau porous structure of an arbitrary cross section shown in Fig. 2(a), it is supposed that the inclined strut l and vertical strut h have the same length (l=h), and their widths are $t(x)=t_0[1+\alpha(2x/l)^2]$ (where $0\le x\le l/2$, t_0 is the width of the struts at the midpoint, and α is a constant larger than zero), the cross-section area is $A(x)= t(x)\cdot b$ and the inertia moment of the cross section is $I(x)= t^3(x)\cdot b/12$. Thus, Eqs. (4), (5), (9), (12), (13) for calculating the effective elastic constants can be simplified as follows:

$$\frac{E_1^*}{E_s}=\frac{E_2^*}{E_s}=\frac{2\sqrt{3}}{3}\cdot\frac{1}{3J_A+2k(1+\mu)\cdot J_A+J_B} \tag{14}$$

$$\frac{G_{12}^*}{E_s}=\frac{\sqrt{3}}{6}\times\frac{1}{J_A+2k(1+\mu)\cdot J_A+J_B} \tag{15}$$

$$\mu_{12}^*=-\frac{J_A-2k(1+\mu)\cdot J_A-J_B}{3J_A+2k(1+\mu)\cdot J_A+J_B} \tag{16}$$

where

$$J_A=b\cdot\int_0^{L_i/2}\frac{\mathrm{d}x}{A(x)}=\frac{l}{t_0}\frac{\arctan\sqrt{\alpha}}{2\sqrt{\alpha}} \tag{17}$$

$$J_B=b\cdot\int_0^{L_i/2}\frac{x^2\mathrm{d}x}{I(x)}=\frac{l^3}{t_0^3}\cdot\frac{3}{8\alpha}\cdot\left[-\frac{1}{(1+\alpha)^2}+\frac{1}{2(1+\alpha)}+\frac{\arctan\sqrt{\alpha}}{2\sqrt{\alpha}}\right] \tag{18}$$

The relative density is

$$\rho=\frac{\rho^*}{\rho_s}=\frac{4\int_0^{l/2}A(x)\mathrm{d}x+2\int_0^{h/2}A(x)\mathrm{d}x}{(h+l\sin\theta)\cdot 2l\cos\theta\cdot b}=\frac{2(3+\alpha)}{3\sqrt{3}}\frac{t_0}{l} \tag{19}$$

Let α=0.5, the width of strut is $t(x)=t_0[1+0.5\times(2x/l)^2]$. Thus, Eqs. (17)−(19) are reduced to

$$J_A=0.4352\frac{l}{t_0} \tag{20}$$

$$J_B=0.2431\frac{l^3}{t_0^3} \tag{21}$$

$$\rho=\frac{7\sqrt{3}}{9}\frac{t_0}{l} \tag{22}$$

By substituting Eqs. (20)−(22) into Eqs. (14)−(16), calculation formulas of the effective elastic constants are obtained for the non-uniform and regular Plateau porous structure:

$$\frac{E_1^*}{E_s}=\frac{E_2^*}{E_s}=\frac{2\sqrt{3}}{3}\cdot\frac{1}{0.4352\left[3+2k(1+\mu)\right]\left(\frac{l}{t_0}\right)+0.2431\left(\frac{l}{t_0}\right)^3}=\frac{0.4723\rho^3}{0.2398\left[3+2k(1+\mu)\right]\rho^2+0.2431} \tag{23}$$

$$\frac{G_{12}^*}{E_s}=\frac{1}{2\sqrt{3}}\cdot\frac{1}{0.4352\left[1+2k(1+\mu)\right]\left(\frac{l}{t_0}\right)+0.2431\left(\frac{l}{t_0}\right)^3}=\frac{0.1181\rho^3}{0.2398\left[1+2k(1+\mu)\right]\rho^2+0.2431} \tag{24}$$

$$\mu_{12}^*=\mu_{21}^*=-\frac{0.4352\left[1-2k(1+\mu)\right]\left(\frac{l}{t_0}\right)-0.2431\left(\frac{l}{t_0}\right)^3}{0.4352\left[3+2k(1+\mu)\right]\left(\frac{l}{t_0}\right)+0.2431\left(\frac{l}{t_0}\right)^3}=-\frac{0.2398\left[1-2k(1+\mu)\right]\rho^2-0.2431}{0.2398\left[3+2k(1+\mu)\right]\rho^2+0.2431} \tag{25}$$

4.2 Effective elastic constants of uniform and regular Plateau porous structure

For the uniform and regular hexagonal porous structure, suppose α=0, thus the width of the strut is $t(x)=t_0$, its cross section area is $A(x)= t_0\cdot b$ and inertia moment of cross section is $I(x)=t_0^3\cdot b/12$. Equations (17)−(19) can be simplified as

$$J_A=\frac{l}{2t_0} \tag{26}$$

$$J_B=\frac{l^3}{2t_0^3} \tag{27}$$

$$\rho=\frac{2\sqrt{3}}{3}\frac{t_0}{l} \tag{28}$$

By substituting Eqs. (26)−(28) into Eqs. (14)− (16), calculation formulas of the effective elastic constants are obtained for the uniform and regular hexagonal porous structure:

$$\frac{E_1^*}{E_s}=\frac{E_2^*}{E_s}=\frac{2\sqrt{3}}{3}\cdot\frac{1}{\frac{3}{2}\left(\frac{l}{t_0}\right)+k(1+\mu)\left(\frac{l}{t_0}\right)+\frac{1}{2}\left(\frac{l}{t_0}\right)^3}=$$

$$\frac{6\rho^3}{9\rho^2+6k(1+\mu)\rho^2+4} \tag{29}$$

$$\frac{G_{12}^*}{E_s}=\frac{1}{2\sqrt{3}}\cdot\frac{1}{\frac{1}{2}\left(\frac{l}{t_0}\right)+k(1+\mu)\left(\frac{l}{t_0}\right)+\frac{1}{2}\left(\frac{l}{t_0}\right)^3}=$$

$$\frac{3\rho^3}{6\rho^2+12k(1+\mu)\rho^2+8} \tag{30}$$

$$\mu_{12}^*=\mu_{21}^*=-\frac{\frac{1}{2}\left(\frac{l}{t_0}\right)-k(1+\mu)\left(\frac{l}{t_0}\right)-\frac{1}{2}\left(\frac{l}{t_0}\right)^3}{\frac{3}{2}\left(\frac{l}{t_0}\right)+k(1+\mu)\left(\frac{l}{t_0}\right)+\frac{1}{2}\left(\frac{l}{t_0}\right)^3}=$$

$$\frac{-3\rho^2+6k(1+\mu)\rho^2+4}{9\rho^2+6k(1+\mu)\rho^2+4} \tag{31}$$

4.3 Comparison of this model with currently-existing models

Non-uniform Plateau porous structure model is used both in this study and Ref. [11] for predicting effective elastic constants of porous materials. Our explicit expressions of effective elastic constants in terms of the macroscopic relative density rather than the microstructural parameters obtained in Ref. [11] are more convenient to engineering application. For uniform and regular Plateau porous structure, our results shown in Eqs. (32)−(34) are the same as those in Ref. [11].

$$\frac{E_1^*}{E_s}=\frac{E_2^*}{E_s}=\frac{2\sqrt{3}}{3}\cdot\frac{1}{\frac{3}{2}\left(\frac{l}{t_0}\right)+\frac{1}{2}\left(\frac{l}{t_0}\right)^3} \tag{32}$$

$$\frac{G_{12}^*}{E_s}=\frac{1}{2\sqrt{3}}\cdot\frac{1}{\frac{1}{2}\left(\frac{l}{t_0}\right)+\frac{1}{2}\left(\frac{l}{t_0}\right)^3} \tag{33}$$

$$\mu_{12}^*=\mu_{21}^*=-\frac{\frac{1}{2}\left(\frac{l}{t_0}\right)-\frac{1}{2}\left(\frac{l}{t_0}\right)^3}{\frac{3}{2}\left(\frac{l}{t_0}\right)+\frac{1}{2}\left(\frac{l}{t_0}\right)^3} \tag{34}$$

In addition, hexagonal cellular model and mechanics model of composite materials are used to predict effective elastic constants of porous materials in Refs. [9] and [15], respectively. Let k=1.2 and μ=1/3 for comparison of our models with the other two models.

Calculation formulas of the effective elastic constants were given in Ref. [9] as follows:

$$\frac{E_1^*}{E_s}=\frac{E_2^*}{E_s}=\frac{4\sqrt{3}}{3}\cdot\frac{\left(\frac{t}{l}\right)^3}{1+(5.4+1.5\mu)\left(\frac{t}{l}\right)^2}$$

$$\frac{G_{12}^*}{E_s}=\frac{\sqrt{3}\left(\frac{t}{l}\right)^3}{3+(9.9+5.25\mu)\left(\frac{t}{l}\right)^2}$$

$$\mu_{12}^*=\mu_{21}^*=\frac{1+(1.4+1.5\mu)\left(\frac{t}{l}\right)^2}{1+(5.4+1.5\mu)\left(\frac{t}{l}\right)^2}$$

Calculation formula of the effective elastic modulus was given in Ref. [15] as follows:

$$\frac{E^*}{E_s}=3.287\rho^{1.905}(7-4\overline{\rho})^{0.179}\frac{5-2\rho}{23-11\rho}$$

Figures 6−8 show variation curves of the effective elastic constants with the relative density (ρ^*/ρ_s) obtained in this study, Refs. [9] and [15]. Our results of E_1^* and G_{12}^* increase with the increase of ρ^*/ρ_s. The larger the relative density, the more the solid material per unit volume, and thus the stronger the resistant ability of the porous material to elastic deformation. When ρ^*/ρ_s is equal to 0 and 1, corresponding to the full air (no solid material) and fully dense material, the Poisson ratio μ_{12}^* is equal to 1 and 0.3−0.5, which results in the decrease of μ_{12}^* with the increase of ρ^*/ρ_s and the tendency to the Poisson ratio of the dense material. The variations of E_1^*, G_{12}^* and μ_{12}^* with ρ^*/ρ_s are consistent with those predicted by Refs. [9] and [15], and also fit well with the actual situation.

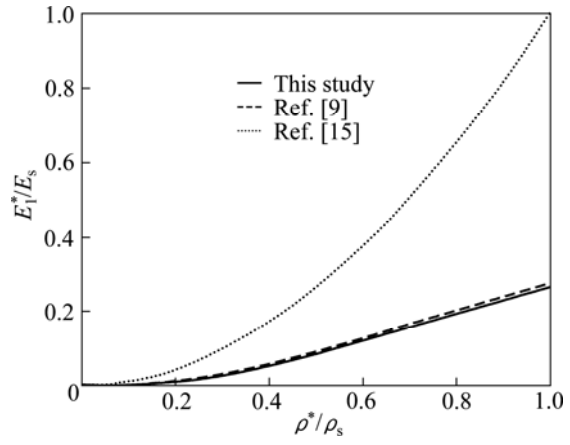

Fig. 6 Variation of E_1^*/E_s with ρ^*/ρ_s

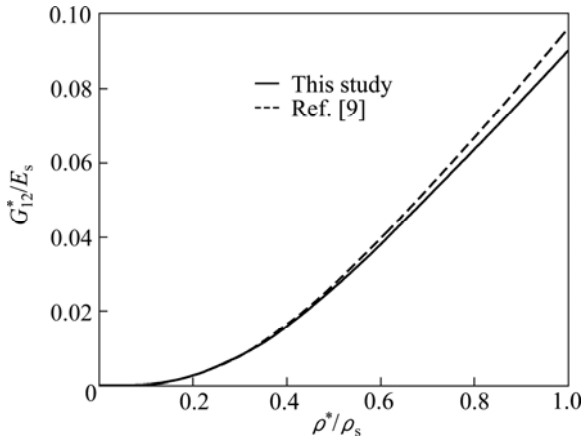

Fig. 7 Variation of G^*_{12}/E_s with ρ^*/ρ_s

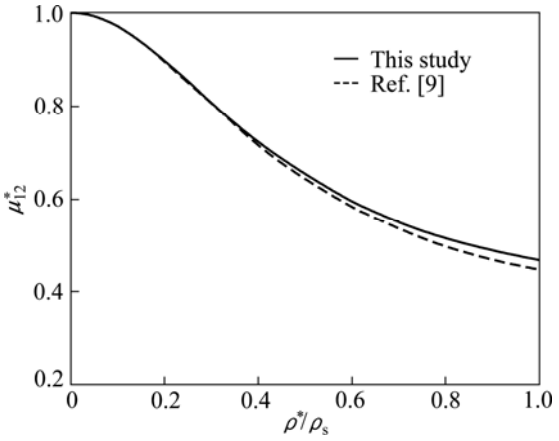

Fig. 8 Variation of μ^*_{12} with ρ^*/ρ_s

Compared with the results in Ref. [9], our results of E^*_1, G^*_{12} and μ^*_{12} are almost the same in the low range of ρ^*/ρ_s. and slightly lower in the medium range of ρ^*/ρ_s and more secure. Effects of axial force, shear force and bending moment on the deformation of Plateau porous structure are taken into account for calculating the effective elastic constants both in Ref. [9] and this study. Geometric method is used in Ref. [9] while energy method is used in our study for calculating the displacement. Obviously, our results are more simple and accurate.

Compared with the results in Ref. [15], our result of E^*_1 is in good agreement with result in Ref. [15] in the low range of ρ^*/ρ_s, but much lower in the medium and high range of ρ^*/ρ_s. That is because mechanics of composite materials is adopted in Ref. [15], where the porous material is regarded as formation of pore and dense body, and the pore's elastic modulus is zero. In nature, effect of the pore distribution and pore interaction on weakening of the elastic modulus of Plateau porous structure cannot be considered, resulting in much higher result of E^*_1. Therefore, Plateau porous structure model established in this study is more reasonable for characterizing the porous material of medium density and more accurate and reliable for predicting its elastic modulus than the composite materials mechanics model.

5 Conclusions

1) A micromechanics model of Plateau porous structure for the new Ti−Al intermetallic compound porous material is established based on microstructure analysis. This model can effectively characterize the open skeleton microstructure and non-uniformity of this new porous material.

2) Calculation formulas of elastic constants (including effective elastic modulus, effective shear elastic modulus and effective Poisson ratio) are derived by the energy method. Results show that both the effective elastic modulus and effective shear elastic modulus increase with the increase of the relative density while the effective Poisson ratio decreases.

3) The explicit expressions of effective elastic constants in terms of the macroscopic relative density obtained in this study are more convenient to engineering application than those in terms of the microstructural parameters obtained in reference.

4) Compared with the currently-existing hexagonal honeycomb model and mechanics model of composite materials, the micromechanics model of heterogeneous Plateau porous structure can take into account the non-uniformity of the microstructure and the effect of the shear on microstructural displacements. Our results of the effective elastic constants obtained by the energy method rather than the geometric method are more accurate for predicting the effective elastic constants of the medium-density porous materials.

References

[1] LETANT S E, HART B R, VAN BUUREN A W, TERMINELLO L J. Functionalized silicon membranes for selective bio-organism capture [J]. Nature Materials, 2003, 2(6): 391−395.

[2] YAMAGUCHI A, UEJO F, YODA T, UCHIDA T, TANAMURA Y, YAMASHITA T. Self-assembly of a silica-surfactant nanocomposite in a porous alumina membrane [J]. Nature Materials, 2004, 3(5): 337−341.

[3] HERNANDEZ N, SANCHEZ-HERENCIA A J, MORENO R. Forming of nickel compacts by a colloidal filtration route [J]. Acta Materialia, 2005, 53(4): 919−925.

[4] van der BRUGGEN B, VANDECASTEELE C. Distillation vs. membrane filtration: Overview of process evolutions in seawater desalination [J]. Desalination, 2002, 143(3): 207−218.

[5] ARIRIATU L E, EWELIKE N C. A low-cost filtration system for the treatment of wastewaters [J]. Environment Protection Engineering, 2003, 29(2): 17−22.

[6] LIU Pei-sheng. Introduction of porous materials [M]. Beijing: Tsinghua University Press, 2004. (in Chinese)

[7] JIANG Yao. Investigation on Ti−Al intermetallic compound porous material [D]. Changsha: Central South University, 2008. (in Chinese)

[8] LI Ting-ting, PENG Chao-qun, WANG Ri-chu, WANG Xiao-feng, LIU Bing, WANG Zhi-yong. Research progress in porous Fe−Al, Ti−A1 and Ni−A1 intermetallic compound porous materials [J]. The Chinese Journal of Nonferrous Metals, 2011, 21(4): 784−795. (in Chinese)

[9] GIBSON L J, ASHBY M F. Cellular solids: Structure and properties [M]. 2nd ed. Cambridge: Cambridge University Press, 1997.

[10] ZHU H X, MILLS N J, KNOTT J F. An analysis of the elastic properties of open-cell foams with tetrakaidecahedral cells [J]. Journal of the Mechanics and Physics of Solids, 1997, 45(3): 319−343.

[11] CHUANG Cheng-Hsin, HUANG Jong-Shin. Elastic moduli and plastic collapse strength of hexagonal honeycombs with plateau borders [J]. International Journal of Mechanical Sciences, 2002, 44: 1827−1844.

[12] LI K, GAO X L, ROY A K. Micromechanics model for three-dimensional open-cell foams using a tetrakaidecahedral unit cell and Castigliano's second theorem [J]. Composites Science and Technology, 2003, 63: 1769−1781.

[13] KIM H S, AL-HASSANI S T S. A morphological elastic model of general hexagonal columnar structures [J]. International Journal of Mechanical Sciences, 2001, 43: 1027−1060.

[14] RAMAKRISHNAN N, ARUNACHALAM V S. Effective elastic moduli of porous solids [J]. Journal of Material Science, 1990, 25: 3930−3937.

[15] LU Zi-xing, HUANG Zhu-ping, WANG Ren. The theoretical prediction of compressive Young's moduli for polyurethane foam plastics [J]. Chinese Journal of Applied Mechanics, 1996, 13(2): 9−12. (in Chinese)

[16] LU Zi-xing, HUANG Zhu-ping, WANG Ren. Determination of effective moduli for foam plastics based on three phase spheroidal model [J]. Chinese Journal of Solid Mechanics, 1996, 17(2): 95−101. (in Chinese)

[17] LONG Yu-qiu, BAO Shi-hua. Structural mechanics I [M]. Beijing: Higher Education Press, 2006. (in Chinese)

新型金属间化合物多孔材料有效弹性常数的理论预测

苏淑兰[1,2]，饶秋华[1]，贺跃辉[3]

1. 中南大学 土木工程学院，长沙 410075；
2. 中南林业科技大学 土木工程与力学学院，长沙 410004；
3. 中南大学 粉末冶金研究院，长沙 410083

摘 要：基于新型 Ti−Al 金属间化合物多孔材料的微结构特征分析，建立了该材料的 Plateau 多孔结构细观力学模型，通过能量法推导出该多孔材料有效弹性常数(含有效弹性模量、有效剪切弹性模量、有效泊松比)的理论预测公式。计算结果表明：有效弹性模量和有效剪切弹性模量均随着相对密度的增加而增加，但有效泊松比随着相对密度的增加而减小。与现有的六边形蜂窝模型及复合材料力学模型相比，非均匀 Plateau 多孔结构细观力学模型更适合于表征中密度多孔材料，更能准确地预测中密度多孔材料的有效弹性常数。现有的非均匀 Plateau 多孔结构模型仅给出有效弹性常数与微观结构参数之间的关系，而本文模型建立了有效弹性常数与宏观相对密度的显式表达式，更方便工程的实际应用。

关键词：金属间化合物；多孔材料；有效弹性常数；Plateau 结构；能量法

(Edited by Hua YANG)